Crystal Field-induced Lattice Expansion upon Reversible Oxygen Uptake/Release in YbMn$_x$Fe$_{2-x}$O$_4$

Tianyu Li[a], Rishvi Jayathilake[a], Lahari Balisetty[a], Yuan Zhang[a], Brandon Wilfong[ab], Timothy Diethrich[a], Efrain Rodriguez*[ab]

[a]Department of Chemistry and Biochemistry, University of Maryland, College Park, Maryland 20742-2115, USA

[b]Maryland Quantum Materials Center, University of Maryland, College Park, Maryland 20742, USA
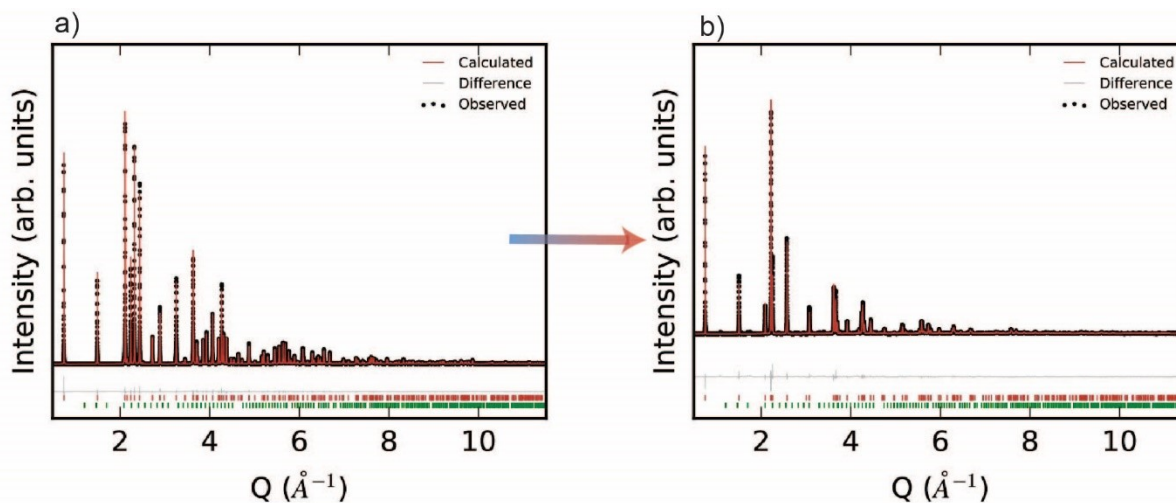
Electronic Supplementary Information

Figures
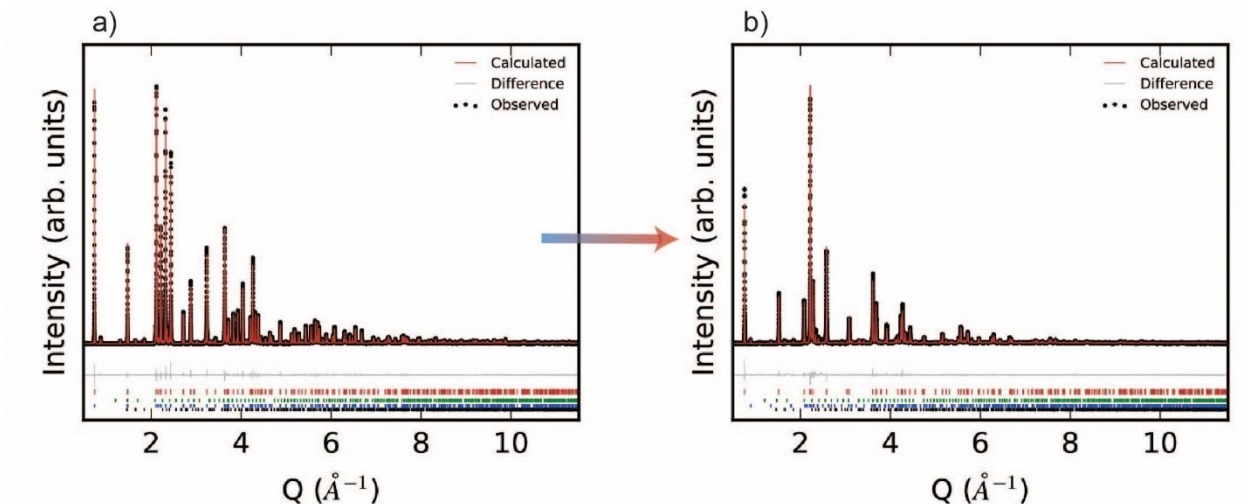
Figure S1. High-resolution synchrotron X-ray powder diffraction pattern and the Rietveld refinement fit of R phase YbMn$_{0.75}$Fe$_{1.25}$O$_4$ (a) and the O phase YbMn$_{0.75}$Fe$_{1.25}$O$_{4.5}$ (b). R phase YbMn$_{0.75}$Fe$_{1.25}$O$_4$ is refined with the $R3m$ symmetry and O phase YbMn$_{0.75}$Fe$_{1.25}$O$_{4.5}$ is refined with the $P3$ symmetry. Small amount of YbMnO$_3$ and Yb$_2$Fe$_3$O$_7$ exists in the samples (indicated by deep blue and cane tick marks)
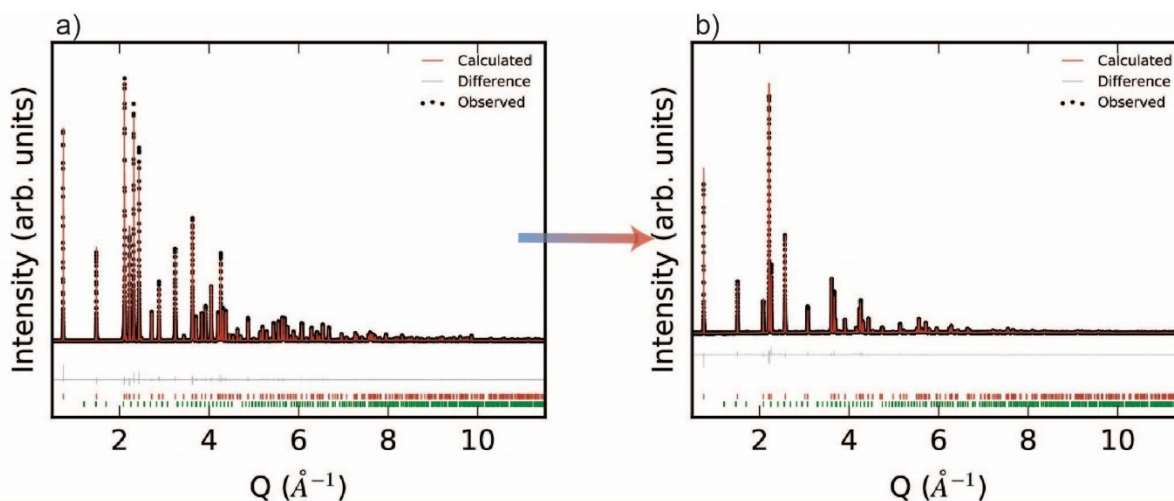
Figure S2. High-resolution synchrotron X-ray powder diffraction pattern and the Rietveld refinement fit of R phase $YbMn_{0.5}Fe_{1.5}O_4$ (a) and the O phase $YbMn_{0.5}Fe_{1.5}O_{4.5}$ (b). R phase $YbMn_{0.5}Fe_{1.5}O_4$ is refined with the $R\bar{3}m$ symmetry and O phase $YbMn_{0.5}Fe_{1.5}O_{4.5}$ is refined with the $P\bar{3}$ symmetry. Small amount of Yb_2O_3 exists in the samples (indicated by green tick marks)


Figure S3. High-resolution synchrotron X-ray powder diffraction pattern and the Rietveld refinement fit of R phase $YbMn_{0.25}Fe_{1.75}O_4$ (a) and the O phase $YbMn_{0.25}Fe_{1.75}O_{4.5}$ (b). R phase $YbMn_{0.25}Fe_{1.75}O_4$ is refined with the $R\bar{3}m$ symmetry and O phase $YbMn_{0.25}Fe_{1.75}O_{4.5}$ is refined with the $P\bar{3}$ symmetry. Small amount of Yb_2O_3 exists in the samples (indicated by green tick marks).
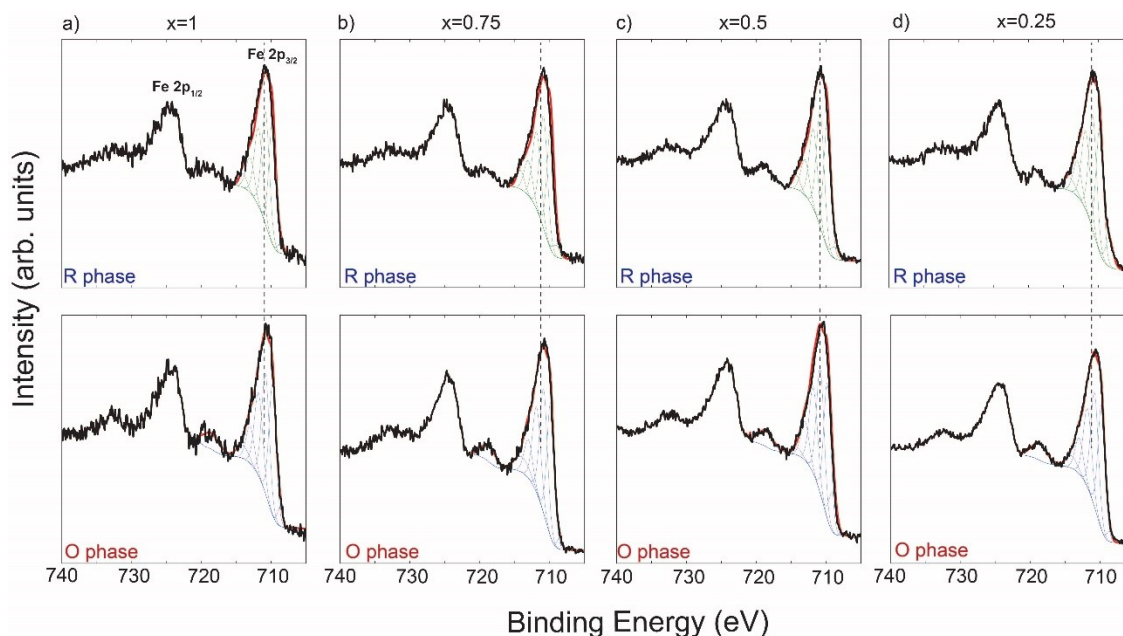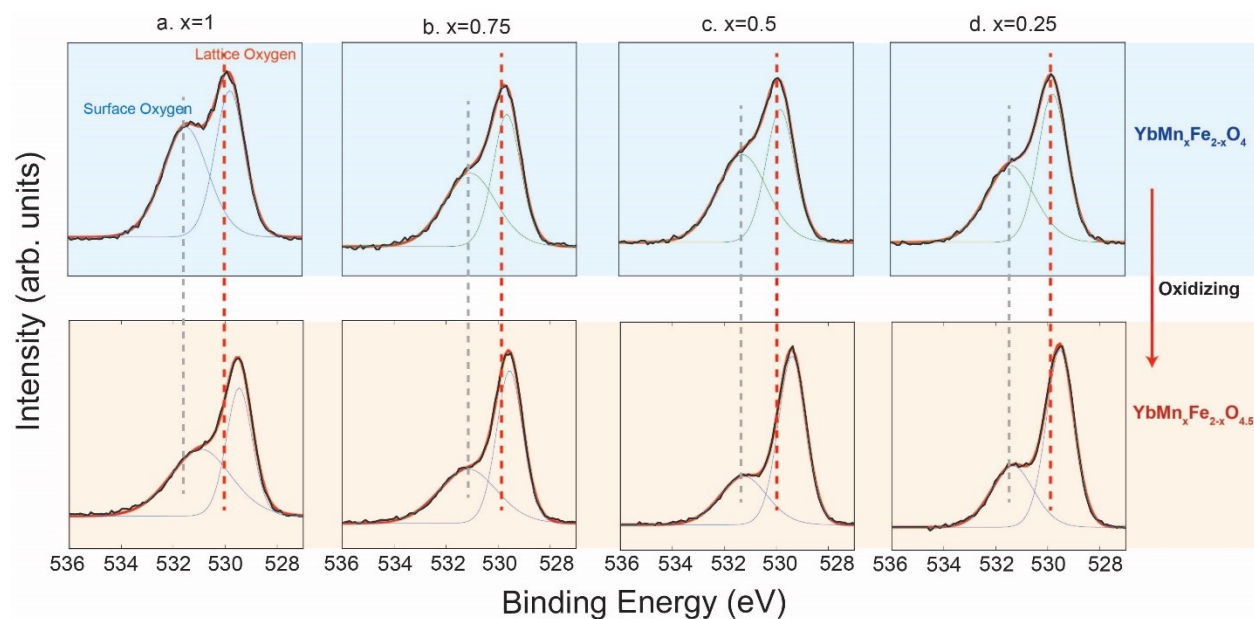
Figure S4. Comparison of Fe 2p XPS spectra between of R phase $YbMn_xFe_{2-x}O_4$ and the O phase $YbMn_xFe_{2-x}O_{4.5}$: a) x=1, b) x=0.75, c) x=0.5, d) x=0.25. Upper figures are the spectra from R phase $YbMn_xFe_{2-x}O_4$. Lower figures are the spectra from O phase $YbMn_xFe_{2-x}O_{4.5}$. All Fe $2p_{3/2}$ spectra can be well fitted with Fe^{3+} profile.
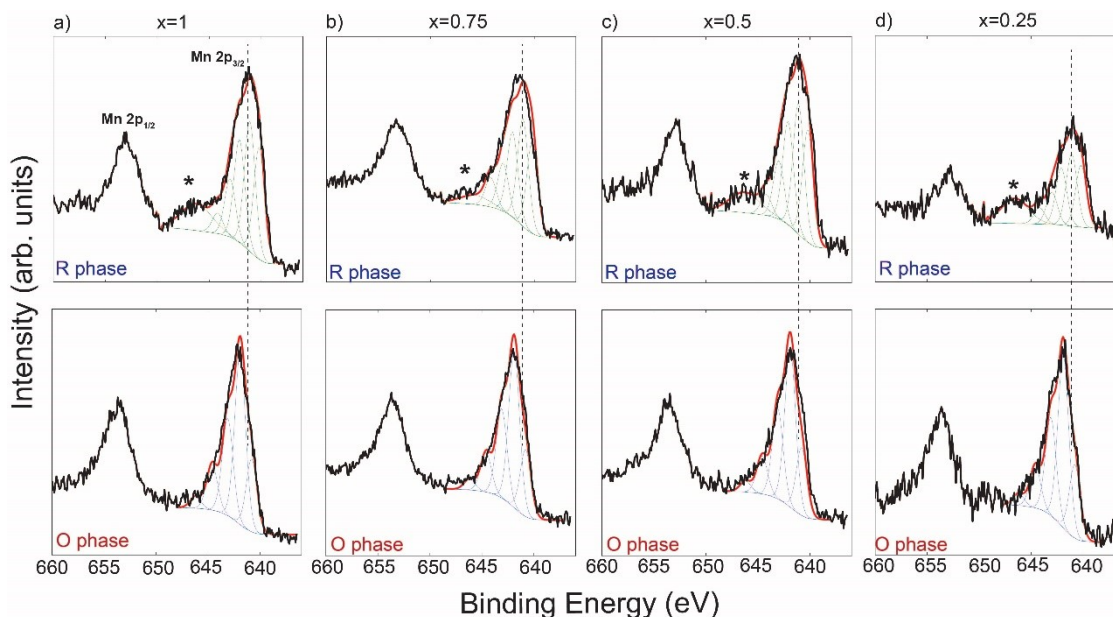
Figure S5. Comparison of Mn 2p XPS spectra between of R phase $YbMn_xFe_{2-x}O_4$ and the O phase $YbMn_xFe_{2-x}O_{4.5}$: a) x=1, b) x=0.75, c) x=0.5, d) x=0.25. Upper figures are the spectra from R phase $YbMn_xFe_{2-x}O_4$. Lower figures are the spectra from O phase $YbMn_xFe_{2-x}O_{4.5}$.

Figure S6. Comparison of O1s XPS spectra between of R phase $YbMn_xFe_{2-x}O_4$ and the O phase $YbMn_xFe_{2-x}O_{4.5}$: a) x=1, b) x=0.75, c) x=0.5, d) x=0.25. Upper figures are the spectra from R phase $YbMn_xFe_{2-x}O_4$. Lower figures are the spectra from O phase $YbMn_xFe_{2-x}O_{4.5}$.
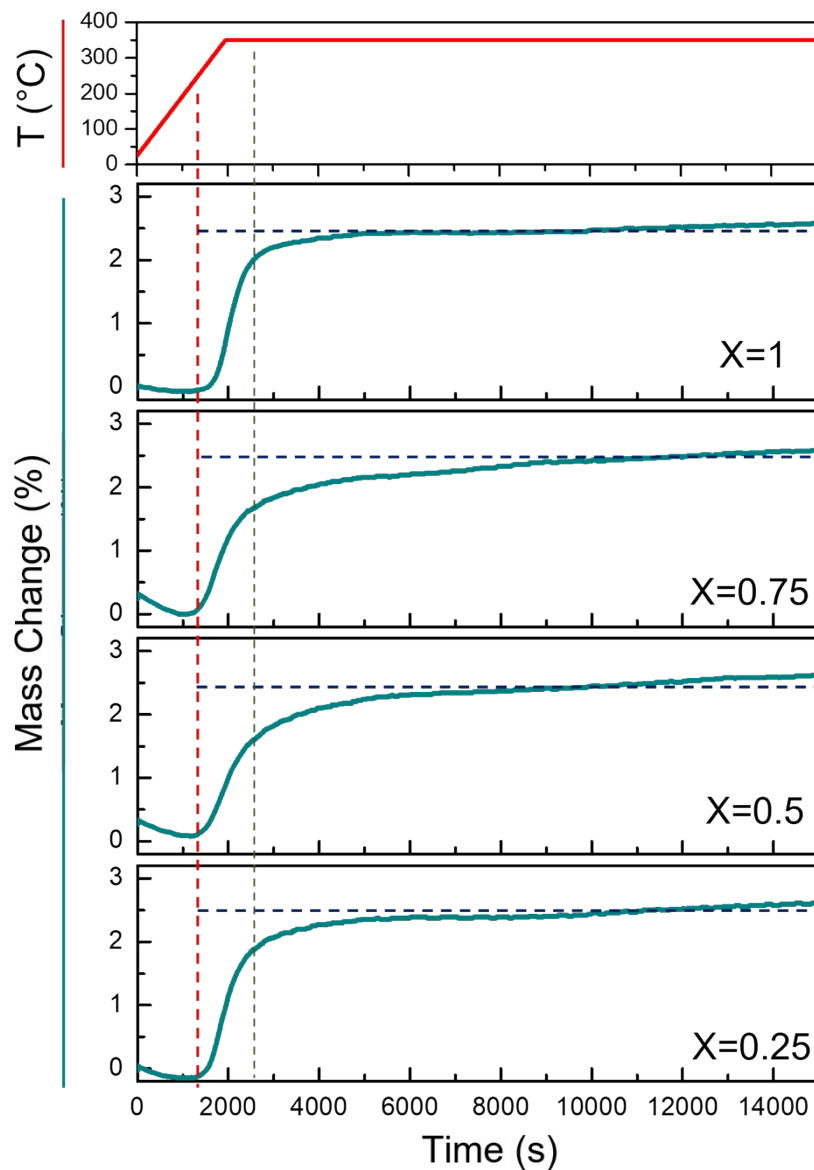
Figure S7. Isotherm heating thermogravimetric analysis (TGA) depicting the weight change as a function of time and temperature for R phases $YbMn_xFe_{2-x}O_4$ in the air.
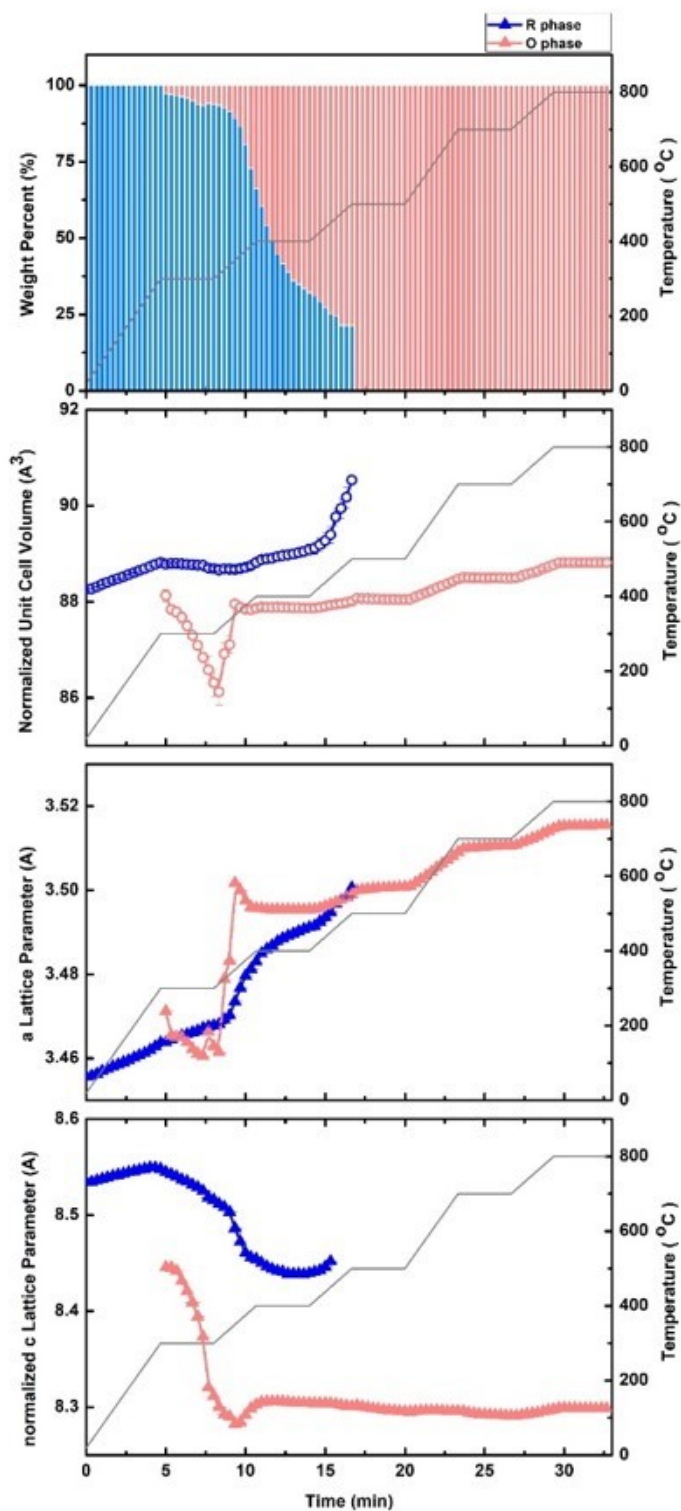
Figure S8. Evolution of phase composition and lattice parameter of R phase YbMn$_x$Fe$_{2-x}$O$_4$ (x=1) during heating in the air.
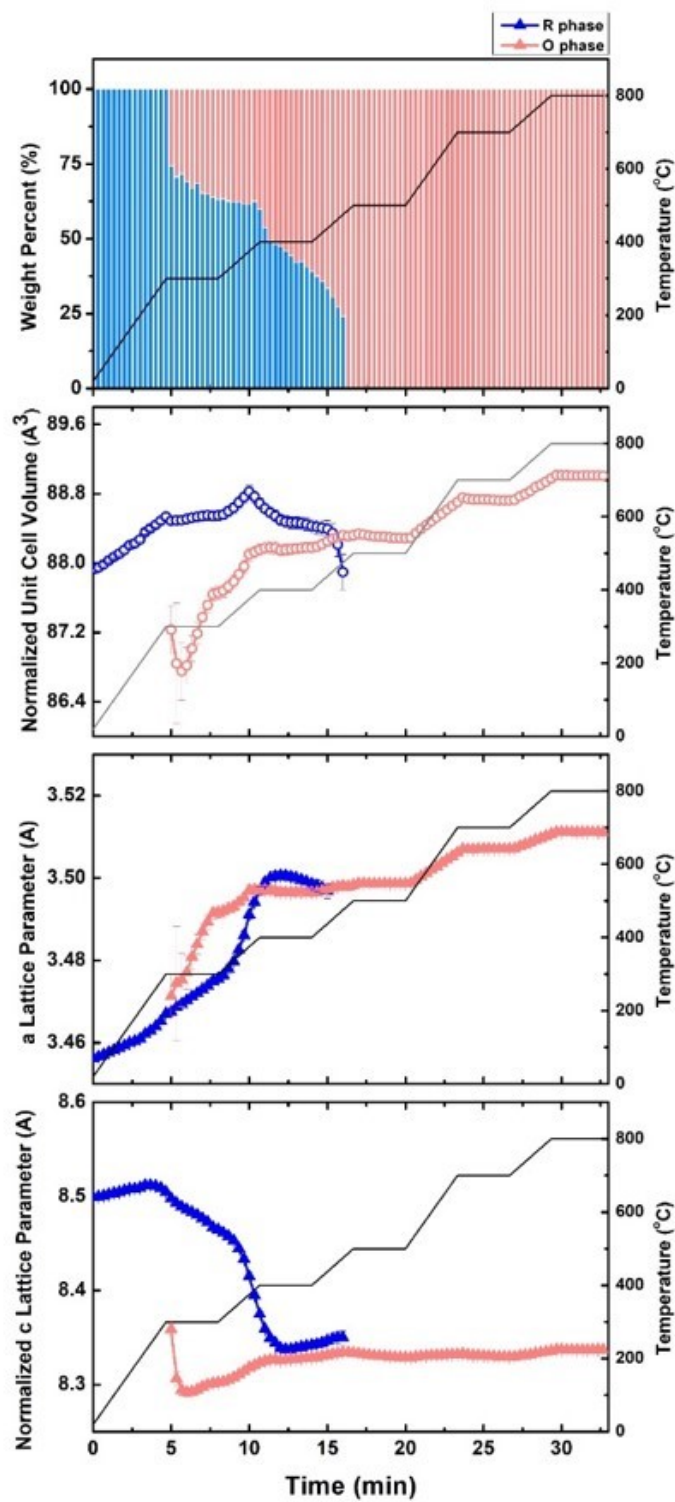
Figure S9. Evolution of phase composition and lattice parameter of R phase YbMn$_x$Fe$_{2-x}$O$_4$ (x=0.75) during heating in the air.
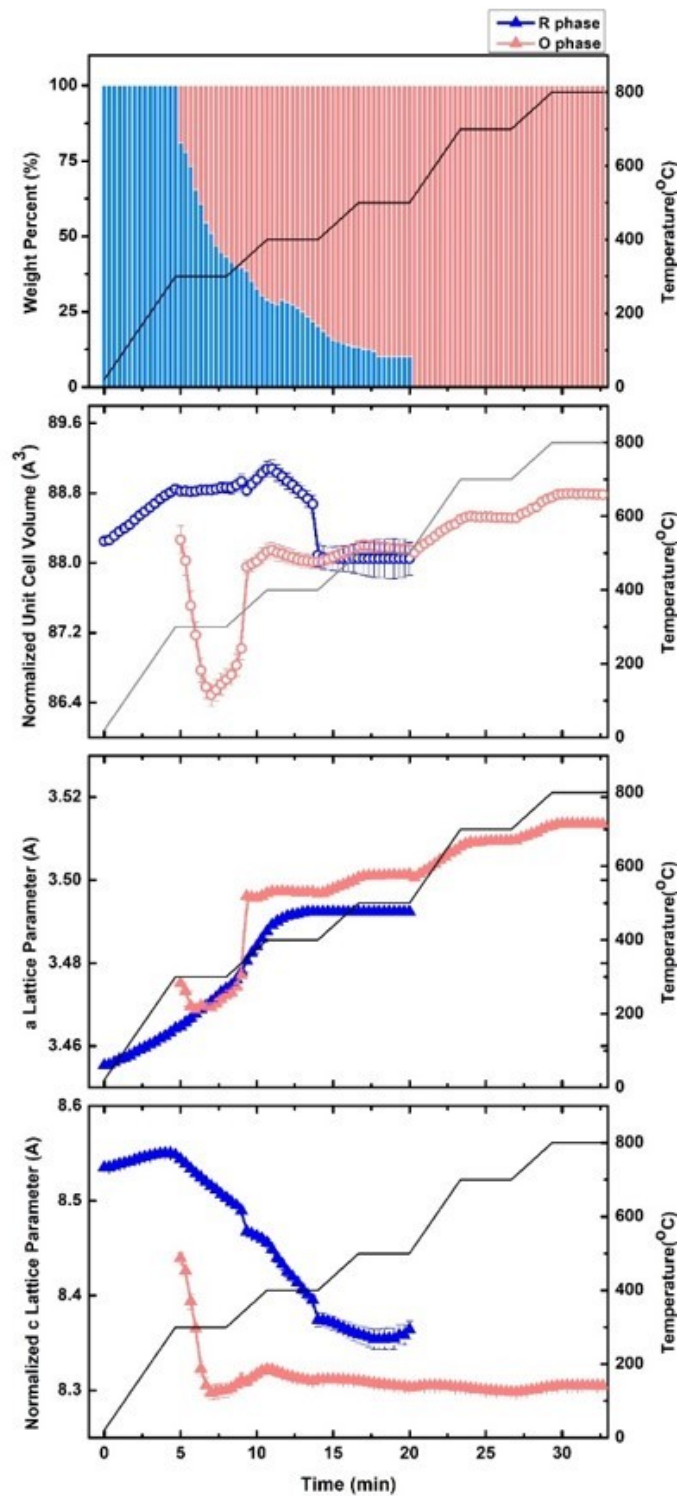
Figure S10. Evolution of phase composition and lattice parameter of R phase YbMn$_x$Fe$_{2-x}$O$_4$ (x=0.5) during heating in the air.
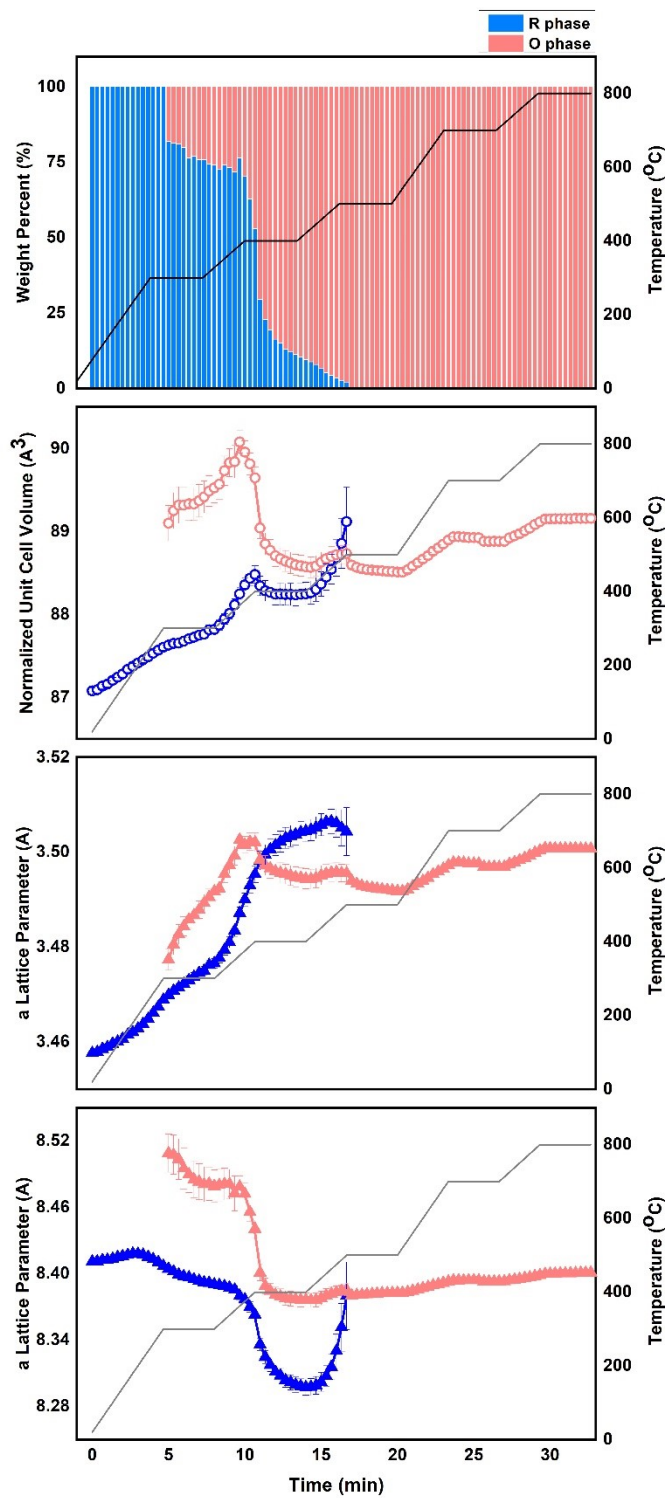
Figure S11. Evolution of phase composition and lattice parameter of R phase YbMn$_x$Fe$_{2-x}$O$_4$ (x=0.25) during heating in the air.
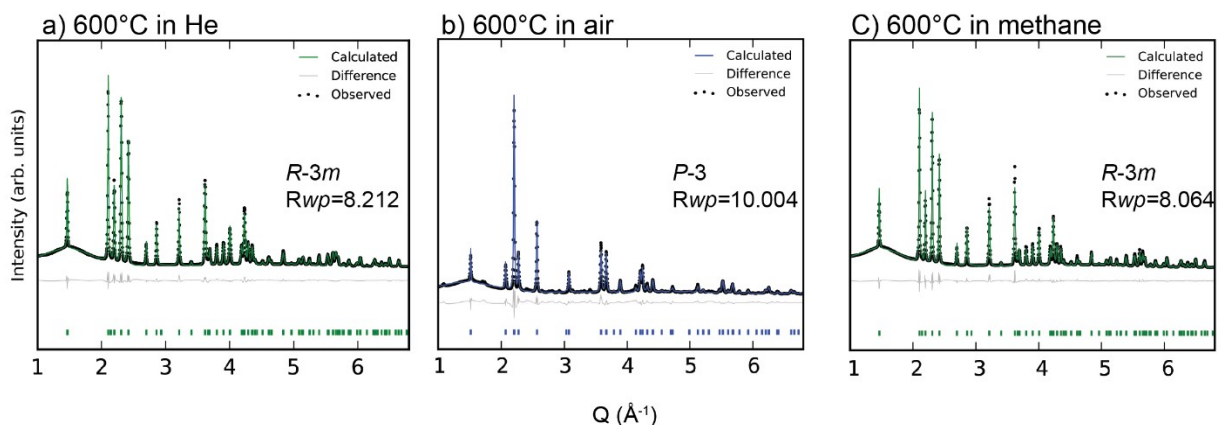
Figure S12. Synchrotron X-ray powder diffraction pattern and the Rietveld refinement fit of a) YbMnFeO$_4$ in He at 600°C. b) YbMnFeO$_4$ in air at 600°C and converted to YbMnFeO$_{4.5.}$ c) O phase YbMnFeO$_{4.5}$ in methane at 600°C and converted back to R phase YbMnFeO$_4$.
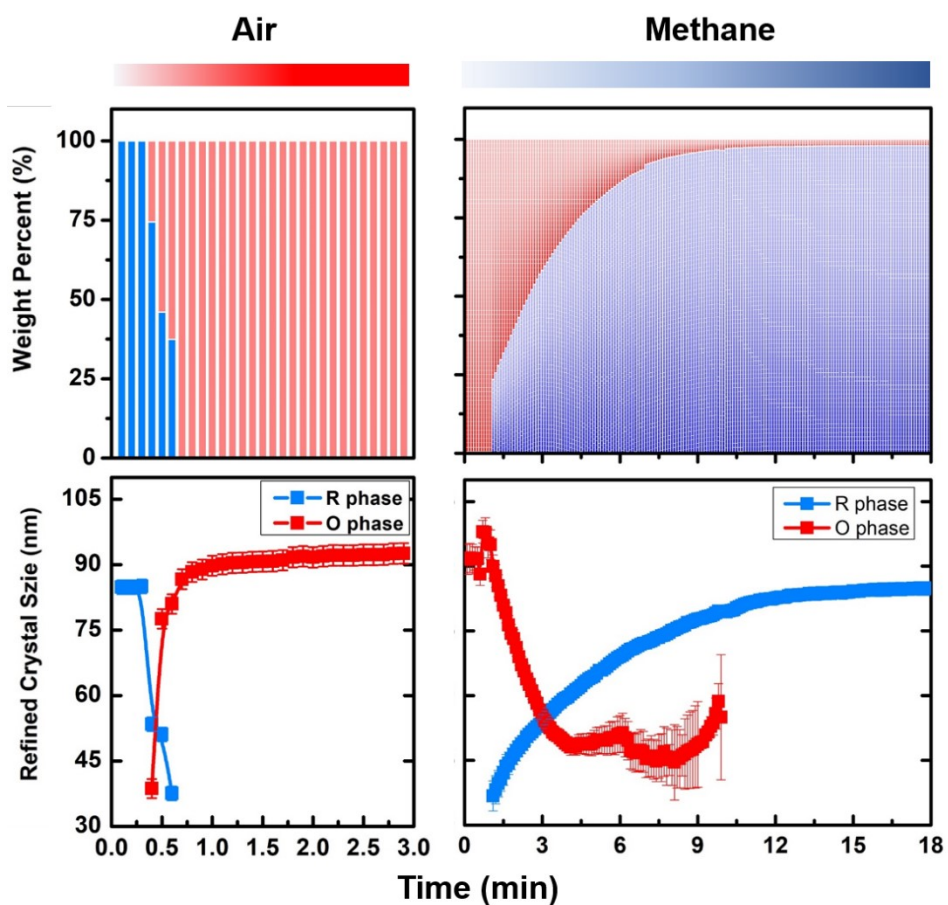
Figure S13. Evolution of phase composition (upper figures) and crystal grain size (lower figures) of YbMnFeO$_4$ during the cycling of air (oxidation) and methane (reduction).

a) Before Cycling
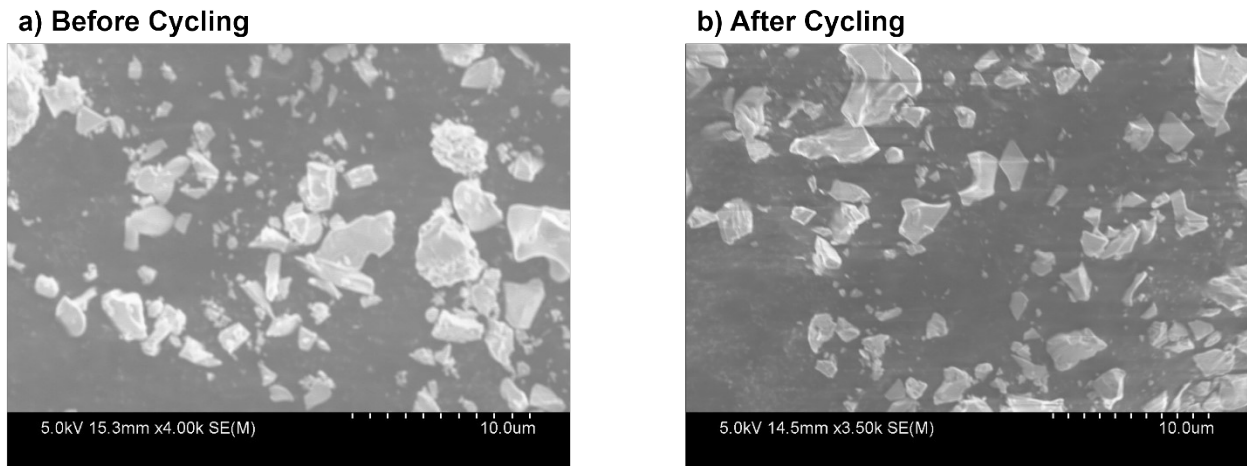
b) After Cycling

Figure S14. SEM image of YbMnFeO$_4$ before and after cycling.

a) Before Cycling
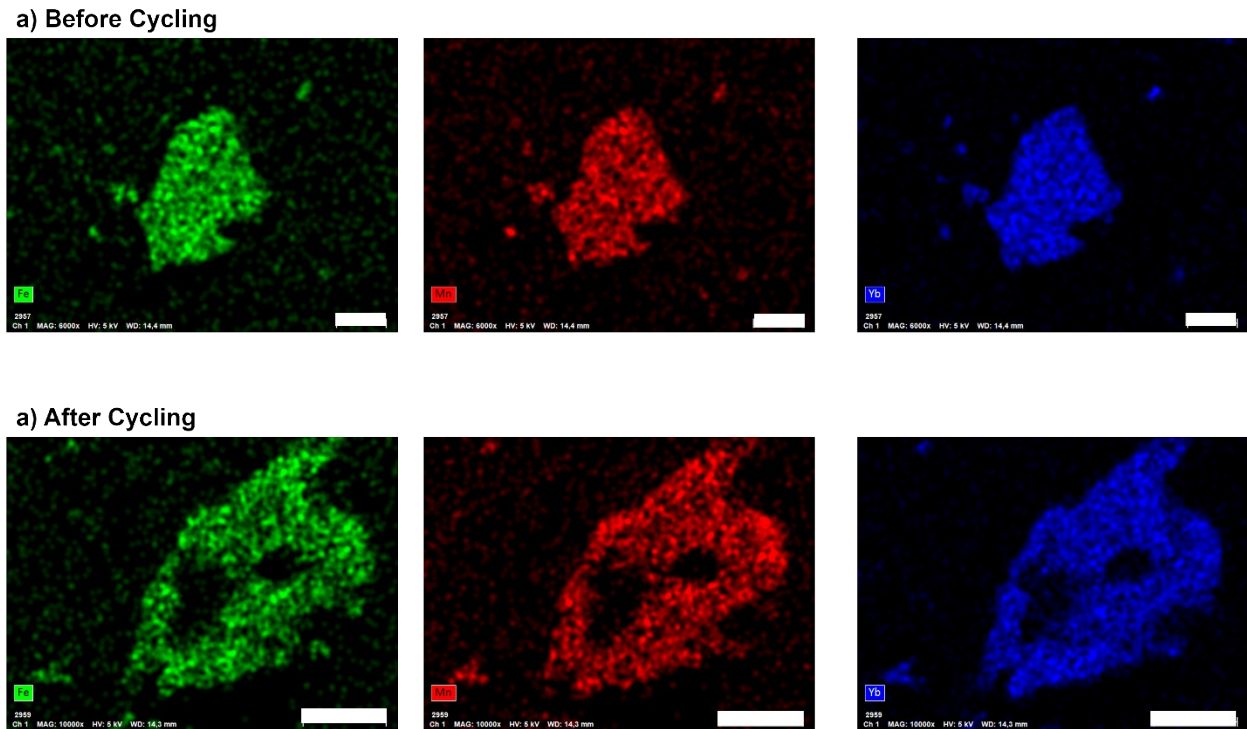
a) After Cycling

Figure S15. SEM-EDS mapping of YbMnFeO$_4$ particle (a) before and (b) after cycling. Scale bar is 2 μm.
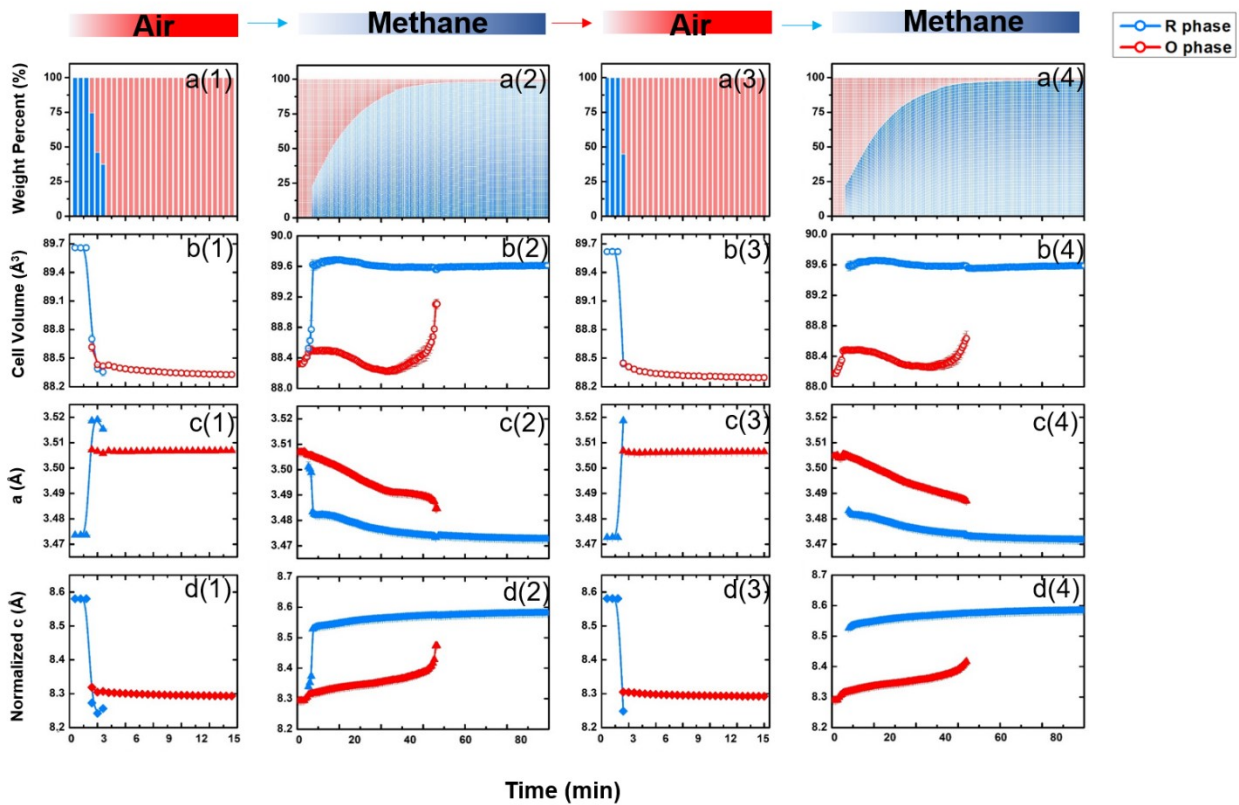
Figure S16. The evolution of a) phase composition, b) crystal cell volume, c) a lattice parameter and d) c lattice parameter as function of time during cycling between oxidizing (air) and reducing (methane) atmospheres at 600 °C for $YbMn_{0.75}Fe_{1.25}O_4$ (x=1).
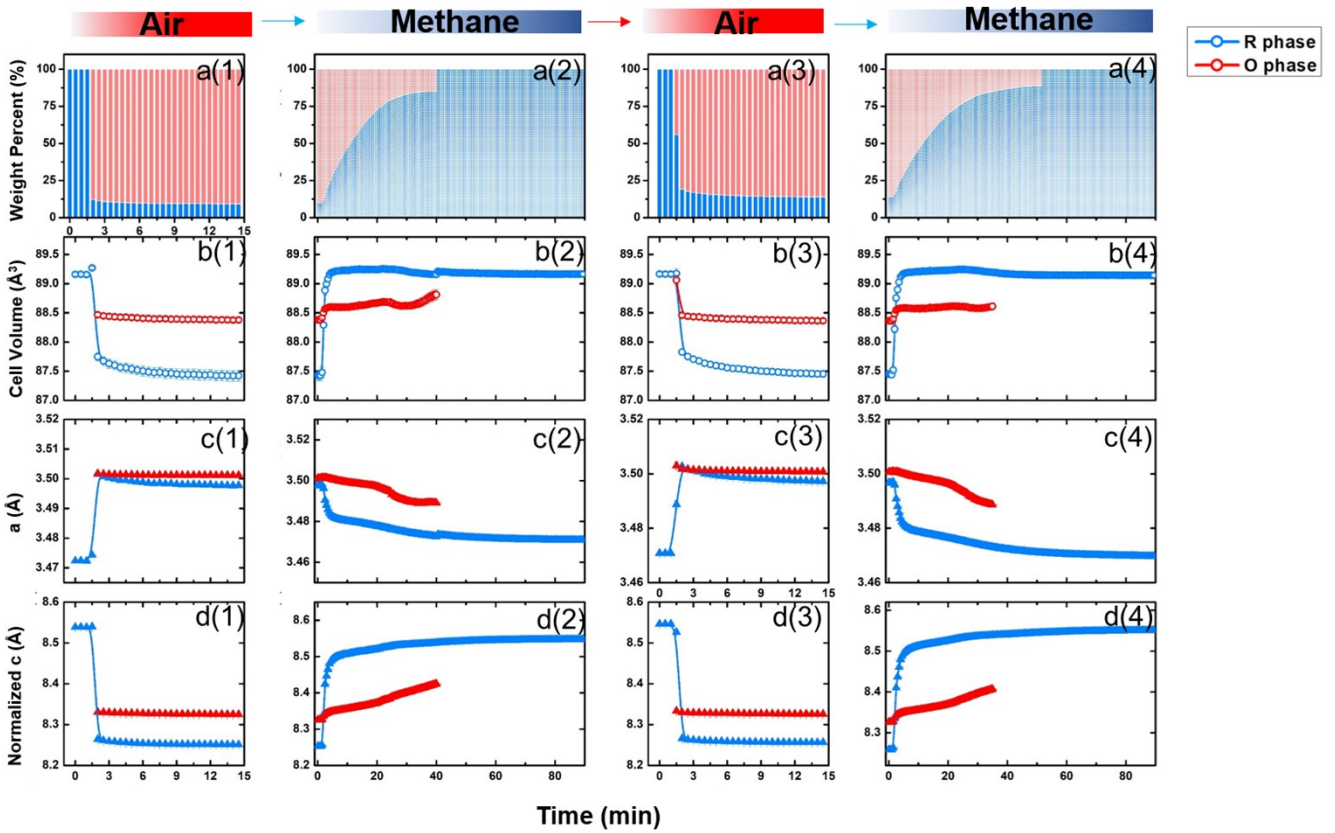
Figure S17. The evolution of a) phase composition, b) crystal cell volume, c) a lattice parameter and d) c lattice parameter as function of time during cycling between oxidizing (air) and reducing (methane) atmospheres at 600 °C for $YbMn_{0.75}Fe_{1.25}O_4$ (x=0.75).
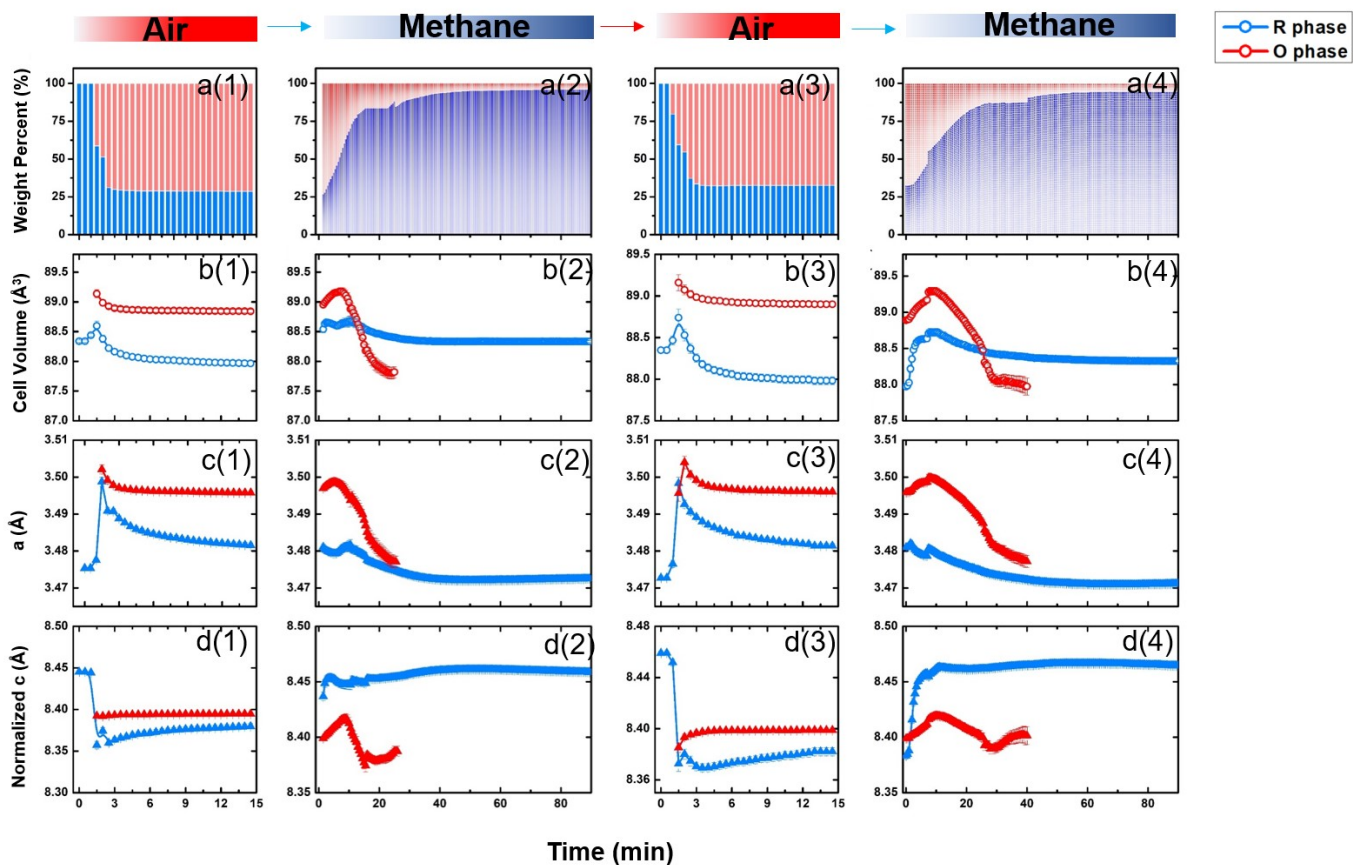
Figure S18. The evolution of a) phase composition, b) crystal cell volume, c) a lattice parameter and d) c lattice parameter as function of time during cycling between oxidizing (air) and reducing (methane) atmospheres at 600 °C for $YbMn_{0.25}Fe_{1.75}O_4$ (x=0.25)
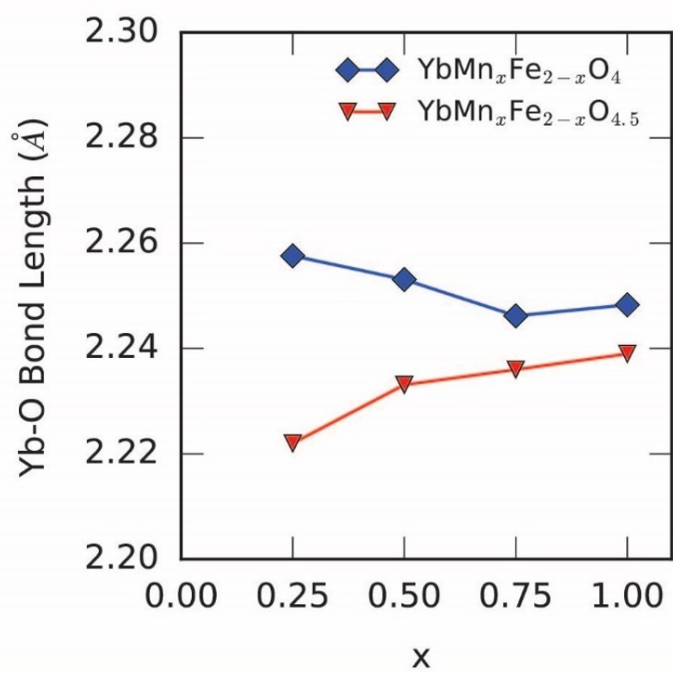
Figure S19. Influence of Mn substitution on Yb-O bond length of R phase YbMn$_x$Fe$_{2-x}$O$_4$ (blue) and the O phase YbMn$_x$Fe$_{2-x}$O$_{4.5}$ (red).
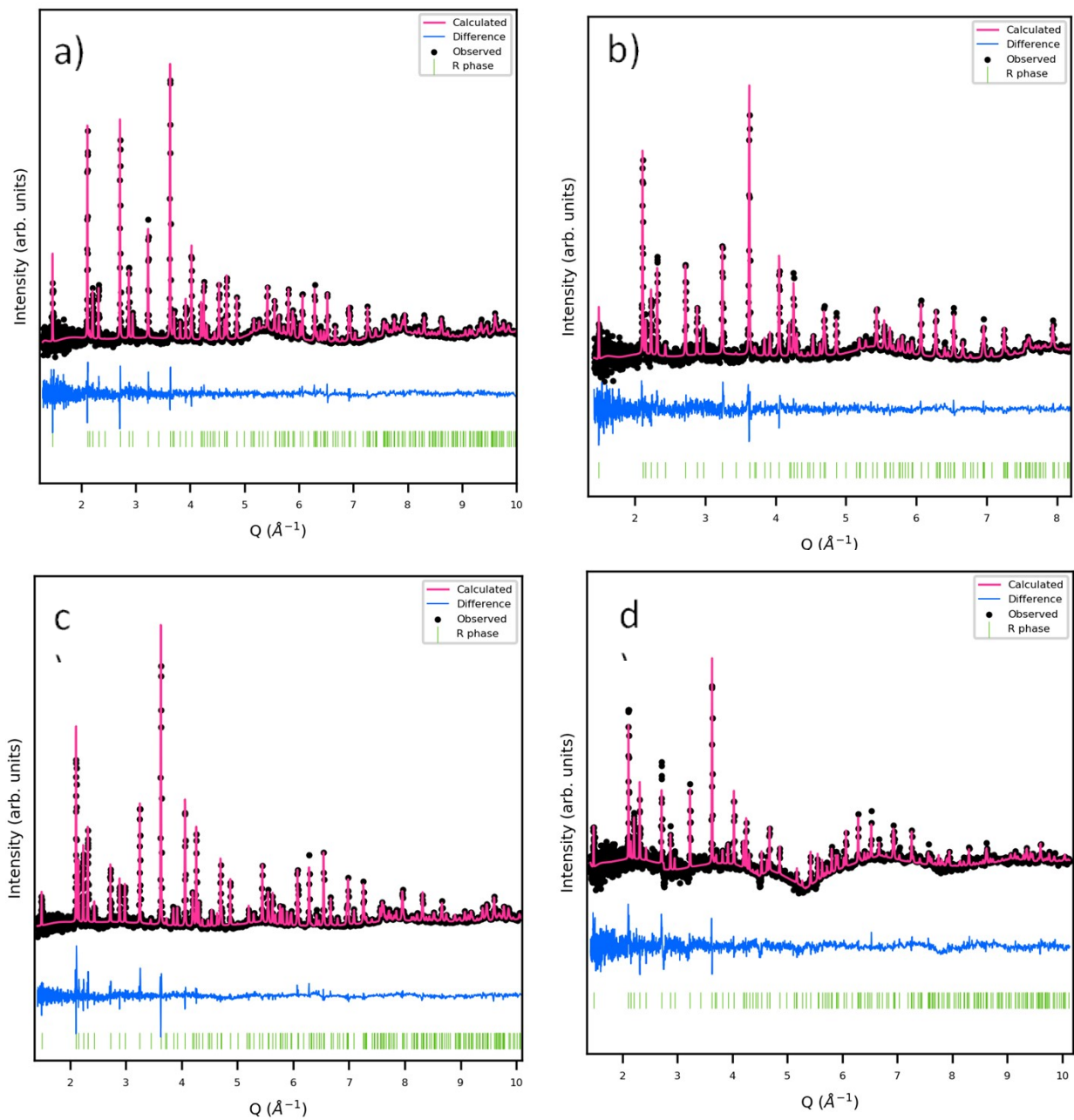
Figure S20. Rietveld refinement of powder neutron diffraction of reduced phases with varying amount of Mn doping: a) $YbMnFeO_4$, b) $YbMn_{0.5}Fe_{1.5}O_4$, c) $YbMn_{0.25}Fe_{1.75}O_4$, d) $YbMn_{0.75}Fe_{1.25}O_4$. Due to that not enough sample were used in the neutron diffraction measurement, the quality of data is poor.

Tables

		atom	occ	x	y	z	u11=u22	u33
YbMnFeO$_4$, *R-3m*								
0.03% Yb$_2$O$_3$		Yb	0.968(1)	0	0	0	0.00180(7)	0.0294(2)
Rwp=10.934%		Fe/Mn	Fe 1/2 Mn 1/2	0	0	0.21578(2)	0.0059(1)	0.0091(3)
a	3.45799(2)	O1	1	0	0	0.12801(7)	beq=1.80(4)	
c	25.6136(1)	O2	0.985(3)	0	0	0.29297(6)	beq=0.62(4)	
YbMn$_{0.75}$Fe$_{1.25}$O$_4$, *R-3m*								
2.61% YbMnO$_3$, 2.15% Yb$_2$Fe$_3$O$_7$		Yb	0.962(2)	0	0	0	0.0035(7)	0.0294(2)
Rwp=8.591%		Fe/Mn	Fe 5/8 Mn 3/8	0	0	0.21577(2)	0.0982(1)	0.0071(2)
a	3.45468(2)	O1	1	0	0	0.1282(1)	beq=2.27(6)	
c	25.5295(2)	O2	0.967(5)	0	0	0.29253(9)	beq=0.86(7)	
YbMn$_{0.5}$Fe$_{1.5}$O$_4$, *R-3m*								
0.48% Yb$_2$O$_3$		Yb	0.9542(1)	0	0	0	0.00275(7)	0.03765(2)
Rwp=11.032%		Fe/Mn	Fe 3/4 Mn 1/4	0	0	0.21551(2)	0.0109(2)	0.0070(3)
a	3.46183(1)	O1	1	0	0	0.12834(8)	beq=2.33(5)	
c	25.4049(1)	O2	0.941(3)	0	0	0.29239(7)	beq=0.80(3)	
YbMn$_{0.25}$Fe$_{1.75}$O$_4$, *R-3m*								
0.32% Yb$_2$O$_3$		Yb	0.956(1)	0	0	0	0.00225(8)	0.0389(2)
Rwp=10.259%		Fe/Mn	Fe 7/8 Mn 1/8	0	0	0.21531(1)	0.0126(2)	0.0106(2)
a	3.46100(1)	O1	1	0	0	0.12815(7)	beq=2.31(4)	
c	25.26212(1)	O2	0.948(4)	0	0	0.29174(7)	beq=0.72(3)	

Table S1. Structural parameters from Rietveld refinement for R phases YbMn$_x$Fe$_{2-x}$O$_4$ (x=1, 0.75, 0.5, 0.25).

YbMnFeO$_{4.5}$, *P-3*
0.03% Yb$_2$O$_3$
Rwp=17.752%

		atom	occ	x	y	z	u11=u22	u33	u12
a	3.48847(2)	Yb	1	0	0	0	0.040(4)	0.0905(7)	0.0050(3)
c	8.24724(8)	Fe/Mn	Fe 1/2 Mn 1/2	0.66666	0.33333	0.3507(2)	0.078(3)	0.0000(8)	0.001(1)
		O1	1	0.66666	0.33333	0.1192(5)	beq=1.6(1)		
		O2	0.385(7)	0	0	0.322(1)	beq=1.0(2)		
		O3	0.865(7)	0.33333	0.66666	0.408(1)	beq=7.4(5)		

YbMn$_{0.75}$Fe$_{1.25}$O$_{4.5}$, *P-3*
2.61% YbMnO$_3$, 2.15% Yb$_2$Fe$_3$O$_7$
Rwp=12.971%

		atom	occ	x	y	z	u11=u22	u33	u12
a	3.47983(2)	Yb	1	0	0	0	0	0.0927(6)	0.0008(3)
c	8.28485(6)	Fe/Mn	Fe 5/8 Mn 3/8	0.66666	0.33333	0.33489(2)	0.076(1)	0.0028(7)	0.001(1)
		O1	1	0.66666	0.33333	0.11050(4)	beq=3.1(1)		
		O2	0.497(7)	0	0	0.3350(6)	beq=0.2(1)		
		O3	0.753(7)	0.33333	0.66666	0.401(6)	beq=0.2(1)		

YbMn$_{0.5}$Fe$_{1.5}$O$_{4.5}$, *P-3*
0.48% Yb$_2$O$_3$
Rwp=12.788%

		atom	occ	x	y	z	u11=u22	u33	u12
a	3.4833699(8)	Yb	1	0	0	0	0.0073(3)	0.0854(4)	0.007(3)
c	8.33177(4)	Fe/Mn	Fe 3/4 Mn 1/4	0.66666	0.33333	0.3495(2)	0.064(2)	0.0000(8)	0.004(1)
		O1	1	0.66666	0.33333	0.1167(4)	beq=1.98(8)		
		O2	0.399(5)	0	0	0.3311(8)	beq=0.7(1)		
		O3	0.851(5)	0.33333	0.66666	0.3995(7)	beq=3.7(2)		

YbMn$_{0.25}$Fe$_{1.75}$O$_{4.5}$, *P-3*
0.48% Yb$_2$O$_3$
Rwp=18.240%

		atom	occ	x	y	z	u11=u22	u33	u12
a	3.47099(1)	Yb	1	0	0	0	0.0021(4)	0.0016(3)	0.0005(3)
c	8.35970(6)	Fe/Mn	Fe 7/8 Mn 1/8	0.66666	0.33333	0.3512(3)	0.064(2)	0.0000(8)	0.00161(1)
		O1	1	0.66666	0.33333	0.1156(6)	beq=2.0(1)		
		O2	0.364(7)	0	0	0.330(1)	beq=1.6(2)		
		O3	0.886(7)	0.33333	0.66666	0.390(1)	beq=3.5(3)		

Table S2. Structural parameters from Rietveld refinement for O phases YbMn$_x$Fe$_{2-x}$O$_{4.5}$ (x=1, 0.75, 0.5, 0.25).

Material $YbMn_xFe_{2-x}O_{4.5}$	Distance (Å)
x=1	2.062(3)
x= 0.75	2.089(6)
x= 0.5	2.095(2)
x=0.25	2.135(4)
*x=0	2.0605

Table S3. Interatomic distances between O2 and O3 in the structure of O phases $YbMn_xFe_{2-x}O_{4.5}$ (x=1, 0.75, 0.5, 0.25,0). *Data for x=0 are from the previous study on $YbFe_2O_{4.5}$[1].

atom	modulation wave component	coefficient		
		x	y	z
YbMnFeO$_{4.5}$				
Yb	Usin (1)	-0.0074	-0.011	0.026
Fe	Usin (1)	0.0567	-0.0507	-0.0108
	Ucos (1)	-0.0147	0.0049	0.0251
super space group: P-1(a,b,g)0				
O1	Usin (1)	-0.3613	0.0374	-0.0111
k=(0.143, 0.2884, 0.0094)	Ucos (1)	0.1205	0.0555	0.06799
Rwp=12.21%				
O2	Usin (1)	0.0237	-0.0432	0.0233
	Ucos (1)	-0.0122	-0.0291	0.0063
O3 (O$_{int}$)	Usin (1)	-0.0257	0.0107	0.0461
	Ucos (1)	0.0155	-0.0277	0.0055
YbMn$_{0.75}$Fe$_{1.25}$O$_{4.5}$				
Yb	Usin (1)	-0.0057	-0.0135	0.0127
Fe	Usin (1)	0.0252	-0.0104	0.0117
	Ucos (1)	0.0547	-0.0051	0.0523
super space group: P-1(a,b,g)0				
O1	Usin (1)	0.0492	0.0431	0.0181
k=(0.1403, 0.29, 0.0098)	Ucos (1)	-0.1039	-0.0612	-0.0093
Rwp=10.64%	O2	Usin (1)	-0.1077	-0.1851	-0.0143
	Ucos (1)	0.0003	-0.0316	0.0067
O3 (O$_{int}$)	Usin (1)	0.0552	0.0414	0.0341
	Ucos (1)	0.0341	-0.0277	-0.0221
YbMn$_{0.5}$Fe$_{1.5}$O$_{4.5}$				
Yb	Usin (1)	-0.0208	-0.0009	0.0126
Fe	Usin (1)	-0.0034	0.0048	0.0091
	Ucos (1)	-0.0305	-0.0135	0.0127
super space group: P-1(a,b,g)0				
O1	Usin (1)	-0.1086	0.0115	0.026
k=(0.1501, 0.2902, 0.0101)	Ucos (1)	-0.2138	0.1101	-0.0121
O2	Usin (1)	0.1921	-0.4905	0.16322
Rwp=10.22%	Ucos (1)	-0.0237	0.0904	0.08248
O3 (O$_{int}$)	Usin (1)	-0.0526	0.0372	-0.0236
	Ucos (1)	0.0561	-0.0603	0.0326
YbMn$_{0.25}$Fe$_{1.75}$O$_{4.5}$				
Yb	Usin (1)	-0.0044	-0.0069	0.0238
Fe	Usin (1)	0.0148	-0.019	0.0061
	Ucos (1)	-0.0011	0.0027	-0.0042
super space group: P-1(a,b,g)0				
O1	Usin (1)	0.0492	0.0431	0.0181
k=(0.1407, 0.2891, 0.0098)	Ucos (1)	-0.1039	-0.0631	-0.0093
Rwp=12.11%	O2	Usin (1)	-0.1077	-0.1851	-0.0143
	Ucos (1)	0.0002	-0.0316	0.0067
O3 (O$_{int}$)	Usin (1)	0.0552	0.0414	-0.0049
	Ucos (1)	0.0341	-0.0221	0.001

Table S4. Modulation parameters of atomic position for O phases $YbMn_xFe_{2-x}O_{4.5}$ (x=1, 0.75, 0.5, 0.25).

Composition	Theoretical oxygen storage capacity (%)	Measured oxygen storage capacity (%) (Step heating/isotherm heating)	Mass used in measurement (mg)
$YbMnFeO_4$	2.300	2.85/2.46	13.27/9.06
$YbMn_{0.75}Fe_{1.25}O_4$	2.299	2.56/2.52	8.93/7.12
$YbMn_{0.5}Fe_{1.5}O_4$	2.297	2.36/2.63	9.21/7.31
$YbMn_{0.25}Fe_{1.75}O_4$	2.296	2.97/2.55	8.63/6.45

Table S5. Theoretical and measured oxygen storage capacity of $YbMn_xFe_{2-x}O_4$ (x=1, 0.75, 0.5, 0.25).

		atom	occ	x	y	z	u11=u22	u33
$YbMnFeO4$, $R\text{-}3m$		Yb	0.93(1)	0	0	0	0.0000(7)	0.037(1)
Rwp = 12.466%		Fe/Mn	0.5	0	0	0.21(1)	0.000(1)	0.00(1)
a	3.4584(4)	O1	1	0	0	0.1273(1)	beq = 2.19(6)	
c	25.5924(6)	O2	0.92(1)	0	0	0.2932(1)	beq = 0.59(4)	
$YbMn_{0.75}Fe_{1.25}O_4$, $R\text{-}3m$		Yb	0.98(3)	0	0	0	0.000(1)	0.017(2)
Rwp = 10.9870028%		Fe/Mn	0.875/0.125	0	0	0.2148(4)	0.0312(2)	0.1113(8)
a	3.45869(7)	O1	1	0	0	0.1283(2)	beq = 1.5(1)	
c	25.554(1)	O2	0.90(2)	0	0	0.2926(3)	beq = 0.3(1)	
$YbMn_{0.5}Fe_{1.5}O_4$, $R\text{-}3m$		Yb	0.96(2)	0	0	0	0.000(1)	0.046(3)
Rwp = 16.2119116%		Fe/Mn	0.75/0.25	0	0	0.2160(2)	0.010(1)	0.012(3)
a	3.46483(6)	O1	1	0	0	0.1276(2)	beq = 2.5(1)	
c	25.3568(9)	O2	0.95(2)	0	0	0.2931(2)	beq = 0.9(1)	
$YbMn_{0.25}Fe_{1.75}O_4$, $R\text{-}3m$		Yb	0.96(1)	0	0	0	0.0000(9)	0.035(1)
Rwp = 12.466%		Fe/Mn	0.875/0.125	0	0	0.2155(1)	0.0094(9)	0.008(1)
a	3.46065(3)	O1	1	0	0	0.1281(1)	beq = 1.68(7)	
c	25.2575(5)	O2	0.97(1)	0	0	0.2929(1)	beq = 0.67(7)	

Table S6: Lattice parameters, atomic coordinates, and displacement parameters of reduced phases at 200 °C from Rietveld fitting of PND data.